Spin Hall magnetoimpedance

Johannes Lotze,[1,2] Hans Huebl,[1,3] Rudolf Gross,[1,2,3] and Sebastian T. B. Goennenwein[1,3]
[1]*Walther-Meißner-Institut, Bayerische Akademie der Wissenschaften, 85748 Garching, Germany*
[2]*Physik-Department, Technische Universität München, 85748 Garching, Germany*
[3]*Nanosystems Initiative Munich (NIM), 80799 München, Germany*
(Received 30 April 2014; revised manuscript received 24 October 2014; published 17 November 2014)

The recently discovered spin Hall magnetoresistance effect electrically probes pure spin current flow across a ferrimagnetic insulator/normal metal bilayer interface. While usually the dc electrical resistance of the bilayer is measured as a function of the magnetization orientation in the magnetic insulator, here we present magnetoimpedance measurements using bias currents with frequencies up to several GHz. We find that the spin Hall magnetoresistance effect is frequency independent up to frequencies of 3 GHz, corroborating the assumption of a frequency-independent spin Hall angle. Our data therefore show that all interaction time constants relevant for the spin Hall magnetoresistance effect are shorter than about 50 ps. Therefore this technique should allow for the fast readout of the magnetization direction in magnetic insulator/normal metal bilayers.

DOI: 10.1103/PhysRevB.90.174419 PACS number(s): 72.25.Mk, 72.25.Pn, 75.47.−m, 75.70.Tj

I. INTRODUCTION

The spin Hall effect (SHE) and its inverse describe the interconversion of charge and spin currents [1]. The SHE thus is of key importance for a broad variety of spin current-based and spin-caloritronic phenomena, such as the spin Seebeck effect [2–8], spin pumping [9–15], and spin Hall magnetoresistance [16–20]. Hereby, it is generally assumed that the spin Hall physics is independent of frequency up to tens or hundreds of GHz. Moreover, even optically detected voltages at THz frequencies [21] have been interpreted in terms of the inverse SHE. Such a fast response of the spin Hall effect appears reasonable, since microscopic models attribute the SHE to spin-orbit coupling. However, an experimental investigation of this conjecture still needs to be put forward.

In order to critically test the presumed frequency independence of spin Hall physics in the GHz frequency range, spin Hall magnetoresistance (SMR) experiments as a function of frequency appear particularly attractive. The SMR arises in ferromagnetic insulator/normal metal (FMI/N) [22] bilayers. A pure spin current is sourced from the charge current flowing in the normal metal by the SHE. Depending on the orientation of the magnetization of the FMI with respect to the spin polarization of the spin current, this spin current can or cannot propagate across the interface into the insulating ferromagnetic layer [23]. This results in a characteristic dependence of the resistance of the normal metal on the magnetization orientation in the adjacent magnetic insulator, although no electrical current flows through the FMI. Owing to this mechanism, the SMR exhibits a characteristic dependence on the magnetization orientation in the FMI, which is qualitatively different from anisotropic magnetoresistance in bulk polycrystalline FM metals [16–19]. Moreover, the SMR depends quadratically on the spin Hall angle θ_{SH} [20], i.e., on spin Hall physics. A possible frequency dependence of the spin Hall angle θ_{SH} should therefore result in a clear frequency dependence in SMR experiments. So far, however, a systematic study of θ_{SH} as a function of frequency is lacking. Although spin pumping experiments have been performed as a function of ferromagnetic resonance frequency [24,25], in these measurements a dc spin current is converted into a measurable dc charge voltage by means of the spin Hall effect. The extracted spin pumping voltage thus reflects the dc spin Hall angle, irrespective of ferromagnetic resonance frequency. In contrast, ac spin pumping experiments [13,14,26] are sensitive to the ac spin Hall angle and the frequency independence of the spin Hall angle at GHz frequencies is implied in the work of Weiler *et al.* [13]. Furthermore, experiments as a function of the ac current frequency allow for testing of the viability of the SHE for high-frequency all-electrical spin current generation, and for SMR-based fast readout of the magnetization orientation of an insulating ferromagnet, which is desirable for use in spintronic devices.

In this paper, we perform magnetoimpedance measurements by applying an ac charge current with frequency $\omega/(2\pi)$ to a yttrium iron garnet/platinum (YIG/Pt) bilayer, and investigate how the resistance $R(\omega,\mathbf{M})$ of the bilayer changes both as a function of frequency, and as a function of the orientation of the magnetization $\mathbf{M}$ in the YIG film. Our data, recorded at room temperature, invariably and quantitatively exhibit the dependence of the resistance on the magnetization orientation characteristic of SMR for charge current frequencies from dc to 3 GHz. In other words, the magnetoresistive response of our YIG/Pt bilayer (viz., the SMR effect) does not depend on frequency to within experimental accuracy up to frequencies of at least 3 GHz. Moreover, our data suggest that the SMR prevails up to 8 GHz (the highest frequency used in our experiment), but a quantitative evaluation is precluded by calibration issues.

II. EXPERIMENTAL

The YIG/Pt bilayer was prepared by growing a 55 nm thick YIG film on a (111)-oriented single-crystalline gadolinium gallium garnet substrate using laser molecular beam epitaxy (MBE) [19,27]. Without breaking the vacuum, the sample was subsequently transferred to an electron beam evaporation chamber and a Pt film with a thickness of 4 nm was deposited onto the YIG. (For more details, see Ref. [19].) For the experiments discussed here, we diced a rectangular piece with lateral dimensions of 2×1.3 mm^2 from the as-grown sample.

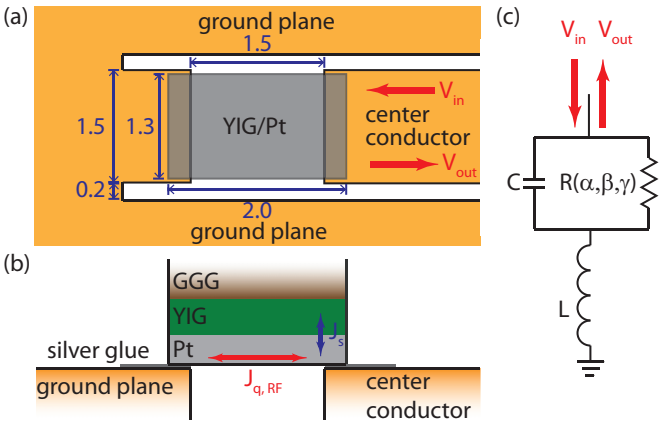

FIG. 1. (Color online) (a), (b) YIG/Pt bilayer bridging a gap in the Cu center conductor of a coplanar waveguide (CPW) structure shown in (a) a top view and (b) a cross-sectional drawing along the center conductor. The dimensions shown are given in mm. (c) The equivalent electrical circuit model used to describe the YIG/Pt bilayer on the CPW.

To measure the impedance of this YIG/Pt sample up to GHz frequencies, we integrate it into a coplanar waveguide (CPW) structure. The latter has a characteristic impedance of 50 Ω and thus allows for the propagation of a high-frequency charge current in a broad frequency range. The CPW structure was patterned onto a printed circuit board (PCB) as shown in Figs. 1(a) and 1(b). The ac current is injected using a surface mount mini-SMP connector at one end of the CPW structure. The CPW is short circuited at the other end. The center conductor is interrupted by a 1.5×1.5 mm^2 square gap in the PCB. The YIG/Pt bilayer is attached to the CPW structure with the Pt facing down toward the copper of the CPW centerline using silver glue, bridging this gap, as shown in Figs. 1(a) and 1(b). Since the sample that is integrated into the CPW structure constitutes a load that is not equal to the system impedance $Z_0 = 50\ \Omega$, part of the ac current is reflected at the sample [28]. Measuring this reflection allows us to extract the impedance of the sample.

The CPW/sample chip is then inserted into the magnetic field of a rotatable electromagnet. We mounted the sample chip in three different ways [see Figs. 2(a), 2(e), and 2(i)]: In the in-plane (ip) configuration, the magnet rotation axis is parallel to the film normal, so that the magnetic field is always in the plane of the YIG/Pt bilayer. The magnetic field direction is parametrized by the angle α between the charge current direction and the magnetic field direction. There are two out-of-plane (oop) configurations: In the oopj configuration the rotation axis of the magnetic field is parallel to the current direction, with the angle β between the magnetic field and the film normal. In the oopt configuration, the rotation axis lies in the film plane, perpendicular to the current direction. The oopt angle γ is enclosed by the magnetic field direction and the film normal. For a (dc) SMR-like behavior [17,19], we expect a $\cos^2(\alpha)$-like resistance modulation with amplitude R_1 on a constant offset R_0 upon rotating the magnetization in the film plane:

$$R_{\mathrm{ip}}(\alpha) = R_0 + R_1 \cos^2\alpha. \tag{1}$$

The ratio

$$\frac{R_1}{R_0} = \frac{2\theta_{\mathrm{SH}}^2\lambda_{\mathrm{SD}}^2\rho t^{-1}G_{\mathrm{r}}\tanh^2\left(\frac{t}{2\lambda_{\mathrm{SD}}}\right)}{1+2\lambda_{\mathrm{SD}}\rho G_{\mathrm{r}}\coth\left(\frac{t}{\lambda_{\mathrm{SD}}}\right)} \tag{2}$$

depends on the spin Hall angle θ_{SH}, the resistivity ρ of the Pt, the spin diffusion length λ_{SD}, the real part of the spin mixing interface conductance G_{r} [20], and the thickness t of the Pt film. As usually done in the literature [16–19], here we take all of these parameters as constants, independent of frequency and magnetic field. We furthermore assume that θ_{SH} is purely

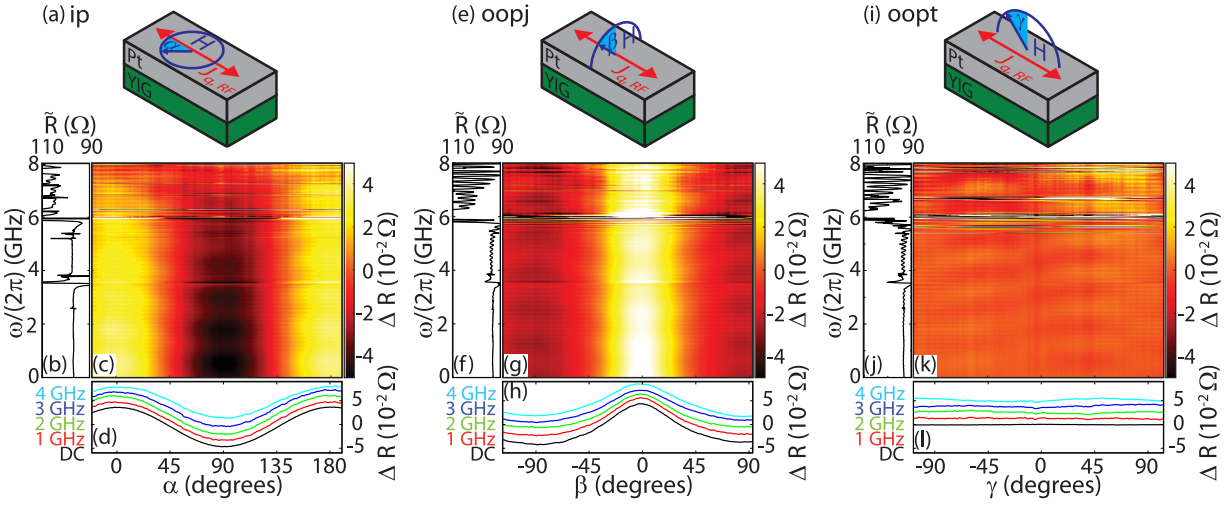

FIG. 2. (Color online) Frequency-dependent resistance for the ip, oopj, and oopt rotation planes. (a), (e), and (i) show a sketch of the YIG/Pt bilayer and the external magnetic field relative to the applied bias current direction. (b), (f), and (j) show $\tilde{R}$ [Eq. (8)] from frequencies of dc to 8 GHz for the respective magnetic field rotations. (c), (g), and (k) show the resistance modulation ΔR with respect to ac current frequency and the corresponding magnetic field rotation angles at a constant external magnetic field of $\mu_0|\mathbf{H}| = 0.6$ T. (d), (h), and (l) show ΔR as a function of the respective rotation angles at different, fixed frequencies: dc (black line), 1 GHz (red line), 2 GHz (green line), 3 GHz (blue line), and 4 GHz (light blue line). The ΔR curves are offset for clarity.

real. For the oopj rotation, we expect

$$R_{\mathrm{oopj}}(\beta) = R_0 + R_1 \cos^2 \beta. \quad (3)$$

In the oopt rotation, the SMR is independent of the magnetization orientation [20] with

$$R_{\mathrm{oopt}} = R_0 + R_1. \quad (4)$$

To establish a reference for the ac resistance measurements, we first measured the dc resistance as a function of the magnetic field orientation at a fixed magnetic field magnitude $\mu_0 H = 0.6$ T for all three magnetic field rotation configurations. In these experiments, a constant bias charge current of 5 mA is applied to the CPW strip and the resistance is calculated from the voltage drop.

In a second set of experiments, we measured the complex reflection coefficient S_{11} at a power level of -5 dBm with an Agilent N5242A vector network analyzer (VNA) as a function of frequency $\omega/(2\pi)$ up to 8 GHz, and as a function of the magnetic field orientation angles α, β, and γ. Again, the magnetic field magnitude hereby was 0.6 T—an external magnetic field sufficiently high as to avoid ferromagnetic resonance. Outside of resonance, both Oersted fields and spin torque generated from the ac current do not have any appreciable impact on magnetization orientation at the power level employed. More precisely, for each measured magnetic field orientation, the frequency of the VNA microwave drive signal is swept, and the corresponding $S_{11}(\omega)$ recorded. Then the magnetic field is rotated to the next orientation, $S_{11}(\omega)$ is recorded, etc. We calibrate the rf circuitry using a set of homemade calibration standards as detailed in the Supplemental Material [29]. The reference measurements with these calibration standards allow us to calibrate the signal path up to the sample position. Ideally, the calibrated S_{11} data then only reflect the properties of the YIG/Pt sample. These homemade calibration standards also introduce a calibration error, as explained in more detail in the Supplemental Material [29].

III. DATA ANALYSIS

The measured calibrated complex scattering parameter S_{11} is converted to the complex impedance Z of the sample via [30]

$$Z(\omega) = \frac{Z_0(1 + S_{11}(\omega))}{1 - S_{11}(\omega)}, \quad (5)$$

where $Z_0 = 50\ \Omega$ is the characteristic impedance of the system. To extract the magnetization orientation-dependent resistance R of the YIG/Pt bilayer from the complex impedance, we use the circuit model sketched in Fig. 1(c). L and C hereby are an inductance and a capacitance, respectively, taken as frequency-independent constants. This model is consistent with models applied to surface mount resistors [31]. The impedance of this L-R-C circuit shown in Fig. 1(c) is given by

$$Z(\omega) = \frac{1}{R\left(C^2\omega^2 + \frac{1}{R^2}\right)} + i\left(\omega L - \frac{C\omega}{C^2\omega^2 + \frac{1}{R^2}}\right). \quad (6)$$

In a first step, we calculate $Z(\omega)$ from the measurement data via Eq. (5). We then simultaneously fit $\mathrm{Re}(Z)$ and $\mathrm{Im}(Z)$ with Eq. (6), using R, L, and C as fit parameters. Since at higher frequencies electrical circuit resonance phenomena occur, which cannot be reproduced by the equivalent circuit model, only the part of $Z(\omega)$ with $\omega/(2\pi) < 3$ GHz is included in the fit.

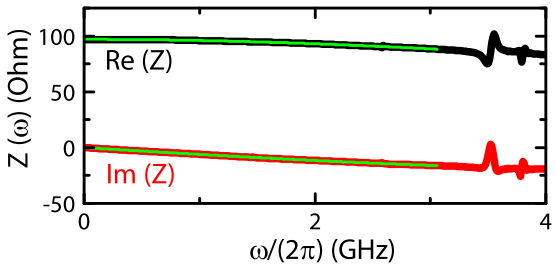

FIG. 3. (Color online) The real and imaginary parts of the complex impedance $Z(\omega)$ recorded for $\mu_0|\mathbf{H}| = 0.6$ T and $\alpha = -90°$ in the ip rotation measurement. Both are fitted simultaneously with Eq. (6) (green line), yielding the capacitance $C = 0.2$ pF and inductance $L = 1$ nH of the equivalent circuit of Fig. 1(c).

This is exemplarily illustrated in Fig. 3, where the real and imaginary parts of the complex impedance as well as the fit according to Eq. (6) (green line) are plotted for the measurement with the external field in the film plane. For both the oopj and oopt rotation the data and fit look very similar. For all three rotation planes we find that $C = 2\times10^{-13}$ F and $L = 1\times10^{-9}$ H consistently describe the data. We did not find L or C to be magnetization orientation dependent. The parameter R is found from the fit to be $R = 97\ \Omega$, corresponding to the measured dc resistance of the device.

The total resistance R consists of two components: the resistance R_0 of the Pt film which is independent of frequency and magnetic field, and R_1, which is magnetization orientation dependent. The (possible) frequency dependence of R_1 is the key focus of this paper. R_1 can be taken as small compared to R_0, because the magnetoresistance ratios R_1/R_0 measured in YIG/Pt are smaller than 10^{-2} [16–19]. Using L and C, we can, in a second step, calculate the magnetization orientation-dependent resistance from the measured impedance by solving Eq. (6) for R:

$$R\left(\omega,\{\alpha,\beta,\gamma\}\right) = \frac{\sqrt{L^2\omega^2 - |Z(\omega,\{\alpha,\beta,\gamma\})|^2}}{\sqrt{C^2\omega^2\left(|Z(\omega,\{\alpha,\beta,\gamma\})|^2 - L^2\omega^2\right) + 2LC\omega^2 - 1}}. \quad (7)$$

$R(\omega,\{\alpha,\beta,\gamma\})$ includes the frequency- and magnetic-field-independent dc resistance R_0 of the platinum and the magnetization orientation-dependent resistance R_1. Since the values of L and C are only reliably determined for frequencies of $\omega/(2\pi) < 3$ GHz, the extraction of $R(\omega)$ at frequencies $\omega/(2\pi) > 3$ GHz cannot be relied on quantitatively.

IV. RESULTS

In Fig. 2, we show the ac magnetoresistance obtained from our measurements for the three rotation planes. This figure is organized as follows: There are four panels for the

three rotation planes, respectively. in Figs. 2(a), 2(e), and 2(i) we show a sketch of each measurement geometry for the three rotation planes and define the rotation angle with respect to the external magnetic field. In Figs. 2(b), 2(f), and 2(j) we show the frequency-dependent resistance averaged over all N magnetization orientations studied in a given magnetic field rotation plane

$$\widetilde{R}(\omega) = \frac{1}{N}\sum_{i=1}^{N} R(\omega,\{\alpha_i,\beta_i,\gamma_i\}) \tag{8}$$

as a function of ac current frequency.

Figures 2(c), 2(g), and 2(k) show the resistance modulation ΔR,

$$\Delta R(\omega,\{\alpha,\beta,\gamma\}) = R(\omega,\{\alpha,\beta,\gamma\}) - \widetilde{R}(\omega), \tag{9}$$

as a function of both frequency and magnetic field angle in a false color plot, while ΔR traces recorded at selected frequencies are depicted in Figs. 2(d), 2(h), and 2(l).

We first analyze the change in dc resistance as a function of the magnetization orientation. The black lines in Figs. 2(d), 2(h), and 2(l) show the change in resistance ΔR(dc) for $\mu_0|\mathbf{H}| = 0.6$ T as a function of the angle. The characteristic $\cos^2(\alpha)$ dependence of Eq. (1) is clearly evident in Fig. 2(d) as well as the expected $\cos^2(\beta)$-type modulation of Eq. (3) for the oopj rotation in Fig. 2(h). In the latter case, the $\cos^2(\beta)$ modulation is not ideal, due to shape anisotropy, which prevents the magnetization from fully aligning with the applied magnetic field when it is not in the sample plane ($\beta = 0^\circ$ corresponds to $\mathbf{H}$ along the film normal; see the Supplemental Material [29]). Last but not least, for a rotation of the 0.6 T magnetic field in the oopt rotation plane, the resistance is constant [Fig. 2(l)], as expected from Eq. (4). Thus the observed angular dependence is the one expected from the SMR effect according to Eqs. (1)–(4). The dc resistance $R_0 = 97\ \Omega$ and a resistance modulation amplitude $R_1 = \max(\Delta R) - \min(\Delta R) = 0.083\ \Omega$ yield a MR ratio of $R_1/R_0 = 8.6\times10^{-4}$. Using the parameters $\theta_{\mathrm{SH}} = 0.11$, $\lambda_{\mathrm{SD}} = 1.5$ nm, $G_{\mathrm{r}} = 4\times10^{14}\ \Omega^{-1}\ \mathrm{m}^2$ [19,32], and the thickness of the Pt film of $t = 4$ nm, one expects a dc SMR magnitude of $R_1/R_0 = 7.7\times10^{-4}$ from Eq. (2), in good agreement to the MR ratio measured experimentally.

We find that the phenomenology of the magnetoresistance observed does not change within experimental accuracy [29] when making the transition from dc to ac bias currents. In the ip rotation of the external magnetic field, shown in Fig. 2(c), we find a modulation of the resistance with a $\cos^2(\alpha)$ dependency, regardless of the ac current frequency, up to at least 3 GHz. Similarly, the oopj data [Fig. 2(g)] show a $\cos^2(\beta)$ dependency, while in the oopt orientation [Fig. 2(k)] the resistance is independent of magnetization orientation. In Figs. 2(d), 2(h), and 2(l), we compare the change in resistance with respect to the applied magnetic field angle at dc as well as 1, 2, 3, and 4 GHz ac currents: The curve shape and the amplitude of the modulation is the same, irrespective of frequency. Qualitatively, this modulation persists at frequencies higher than 3 GHz.

We thus find that the phenomenology of the SMR can be described up to frequencies of at least 3 GHz with real, frequency-independent values for L, C, R, as well as θ_{SH}, of which only the resistance R is magnetization orientation dependent.

V. CONLUSIONS AND SUMMARY

The fact that the SMR effect persists up to at least $\omega/(2\pi) = 3$ GHz means that the interaction time constants $\tau = 1/\omega$ relevant for the SMR effect are shorter than 53 ps. Since the SMR requires both the spin Hall effect and spin torque transfer [20,33,34], i.e., spin-orbit interaction, this can be compared with the spin-orbit interaction time τ_{SO} in platinum. In the free electron model $(2\pi\tau_{\mathrm{SO}})^{-1}$ is estimated to be in the hundreds of GHz [35], and much shorter τ_{SO} are inferred from spin injection, viz., spin transport experiments [36]. A constant SMR magnitude up to tens of GHz thus appears reasonable. From a more applied perspective, our experiments show that the SMR can be used to read out the orientation in a ferromagnetic insulator such as YIG electrically in about 50 ps.

In summary, we have measured the SMR effect in a YIG/Pt bilayer, using currents with frequencies from dc up to 8 GHz. We can describe our results with a simple L-R-C circuit model with frequency-independent constants, of which only the resistance R is magnetization dependent. We find a SMR amplitude (magnetoresistance ratio) of 8.6×10^{-4}, which is unaltered from dc up to frequencies of several GHz. This implies that the spin Hall physics and θ_{SH} in particular enabling the SMR effect are frequency independent within experimental accuracy up to frequencies of at least 3 GHz. This is consistent with theoretical work proposing that the time constants of the SMR should be governed by the spin-orbit interaction.

ACKNOWLEDGMENTS

We thank Stephan Geprägs and Stephan Altmannshofer for the fabrication of the YIG/Pt bilayer. Financial support by Deutsche Forschungsgemeinschaft via Priority Programme "Spin Caloric Transport" SPP 1538 (Project No. GO 944/4-1) is gratefully acknowledged.

[1] J. E. Hirsch, Phys. Rev. Lett. **83**, 1834 (1999).
[2] K. Uchida, H. Adachi, T. Ota, H. Nakayama, S. Maekawa, and E. Saitoh, Appl. Phys. Lett. **97**, 172505 (2010).
[3] M. Weiler, M. Althammer, F. D. Czeschka, H. Huebl, M. S. Wagner, M. Opel, I.-M. Imort, G. Reiss, A. Thomas, R. Gross, and S. T. B. Goennenwein, Phys. Rev. Lett. **108**, 106602 (2012).
[4] M. Schreier, A. Kamra, M. Weiler, J. Xiao, G. E. W. Bauer, R. Gross, and S. T. B. Goennenwein, Phys. Rev. B **88**, 094410 (2013).

[5] S. Hoffman, K. Sato, and Y. Tserkovnyak, Phys. Rev. B **88**, 064408 (2013).
[6] D. Meier, T. Kuschel, L. Shen, A. Gupta, T. Kikkawa, K. Uchida, E. Saitoh, J.-M. Schmalhorst, and G. Reiss, Phys. Rev. B **87**, 054421 (2013).
[7] D. Qu, S. Y. Huang, J. Hu, R. Wu, and C. L. Chien, Phys. Rev. Lett. **110**, 067206 (2013).
[8] S. M. Rezende, R. L. Rodríguez-Suárez, R. O. Cunha, A. R. Rodrigues, F. L. A. Machado, G. A. Fonseca Guerra, J. C. Lopez Ortiz, and A. Azevedo, Phys. Rev. B **89**, 014416 (2014).
[9] Y. Kajiwara, K. Harii, S. Takahashi, J. Ohe, K. Uchida, M. Mizuguchi, H. Umezawa, H. Kawai, K. Ando, K. Takanashi, S. Maekawa, and E. Saitoh, Nature (London) **464**, 262 (2010).
[10] O. Mosendz, J. E. Pearson, F. Y. Fradin, G. E. W. Bauer, S. D. Bader, and A. Hoffmann, Phys. Rev. Lett. **104**, 046601 (2010).
[11] L. H. Vilela-Leão, G. L. da Silva, C. Salvador, S. M. Rezende, and A. Azevedo, J. Appl. Phys. **109**, 07C910 (2011).
[12] C. H. Du, H. L. Wang, Y. Pu, T. L. Meyer, P. M. Woodward, F. Y. Yang, and P. C. Hammel, Phys. Rev. Lett. **111**, 247202 (2013).
[13] M. Weiler, J. M. Shaw, H. T. Nembach, and T. J. Silva, Phys. Rev. Lett. **113**, 157204 (2014).
[14] D. Wei, M. Obstbaum, M. Ribow, C. H. Back, and G. Woltersdorf, Nat. Commun. **5**, 3768 (2013).
[15] C. Hahn, G. de Loubens, M. Viret, O. Klein, V. V. Naletov, and J. Ben Youssef, Phys. Rev. Lett. **111**, 217204 (2013).
[16] N. Vlietstra, J. Shan, V. Castel, B. J. van Wees, and J. Ben Youssef, Phys. Rev. B **87**, 184421 (2013).
[17] C. Hahn, G. de Loubens, O. Klein, M. Viret, V. V. Naletov, and J. Ben Youssef, Phys. Rev. B **87**, 174417 (2013).
[18] H. Nakayama, M. Althammer, Y.-T. Chen, K. Uchida, Y. Kajiwara, D. Kikuchi, T. Ohtani, S. Geprägs, M. Opel, S. Takahashi, R. Gross, G. E. W. Bauer, S. T. B. Goennenwein, and E. Saitoh, Phys. Rev. Lett. **110**, 206601 (2013).
[19] M. Althammer, S. Meyer, H. Nakayama, M. Schreier, S. Altmannshofer, M. Weiler, H. Huebl, S. Geprägs, M. Opel, R. Gross, D. Meier, C. Klewe, T. Kuschel, J.-M. Schmalhorst, G. Reiss, L. Shen, A. Gupta, Y.-T. Chen, G. E. W. Bauer, E. Saitoh, and S. T. B. Goennenwein, Phys. Rev. B **87**, 224401 (2013).
[20] Y.-T. Chen, S. Takahashi, H. Nakayama, M. Althammer, S. T. B. Goennenwein, E. Saitoh, and G. E. W. Bauer, Phys. Rev. B **87**, 144411 (2013).
[21] T. Kampfrath, M. Battiato, P. Maldonado, G. Eilers, J. Nötzold, S. Mährlein, V. Zbarsky, F. Freimuth, Y. Mokrousov, S. Blügel, M. Wolf, I. Radu, P. M. Oppeneer, and M. Münzenberg, Nat. Nanotechnol. **8**, 256 (2013).
[22] For the sake of simplicity, we use the term "ferromagnetic" in the sense of "exhibiting long-range magnetic order." In particular, we also refer to ferrimagnetic materials as ferromagnetic.
[23] Note that although no charge current flows in ferri- or ferromagnetic insulators, a spin current can still propagate in an insulator via magnon (spin wave) propagation.
[24] O. Mosendz, V. Vlaminck, J. E. Pearson, F. Y. Fradin, G. E. W. Bauer, S. D. Bader, and A. Hoffmann, Phys. Rev. B **82**, 214403 (2010).
[25] V. Castel, N. Vlietstra, B. J. van Wees, and J. B. Youssef, Phys. Rev. B **86**, 134419 (2012).
[26] C. Hahn, G. de Loubens, M. Viret, O. Klein, V. V. Naletov, and J. Ben Youssef, Phys. Rev. Lett. **112**, 179901(E) (2014).
[27] M. Opel, J. Phys. D: Appl. Phys. **45**, 033001 (2012).
[28] Note that although the charge current injected into the Pt layer is not necessarily homogeneous, this should not impact the measurement of the magnetoresistance since the magnetoresistance does not depend on charge current density .
[29] See Supplemental Material at http://link.aps.org/supplemental/10.1103/PhysRevB.90.174419. Section A provides details on the calibration procedure and experimental accuracy. Section B provides a calculation of the magnetization orientation as a function of the applied magnetic field angle.
[30] D. Pozar, *Microwave Engineering*, 4th ed. (Wiley, Hoboken, NJ, 2011).
[31] D. Sengupta and V. Liepa, *Applied Electromagnetics and Electromagnetic Compatibility*, Wiley Series in Microwave and Optical Engineering (Wiley, Hoboken, NJ, 2005).
[32] M. Weiler, M. Althammer, M. Schreier, J. Lotze, M. Pernpeintner, S. Meyer, H. Huebl, R. Gross, A. Kamra, J. Xiao, Y.-T. Chen, H. J. Jiao, G. E. W. Bauer, and S. T. B. Goennenwein, Phys. Rev. Lett. **111**, 176601 (2013).
[33] P. M. Haney, H.-W. Lee, K.-J. Lee, A. Manchon, and M. D. Stiles, Phys. Rev. B **87**, 174411 (2013).
[34] P. M. Haney, H.-W. Lee, K.-J. Lee, A. Manchon, and M. D. Stiles, Phys. Rev. B **88**, 214417 (2013).
[35] J. Sakurai, *Modern Quantum Mechanics* (Addison-Wesley, Reading, Massachusetts, 1994).
[36] S. Takahashi and S. Maekawa, Sci. Tech. Adv. Mater. **9**, 014105 (2008).